Second-harmonic generation and multiple mode effects in aperiodic optical superlattices with finite lateral width

2003 J. Phys.: Condens. Matter 15 4889

(http://iopscience.iop.org/0953-8984/15/29/301)

INSTITUTE OF PHYSICS PUBLISHING JOURNAL OF PHYSICS: CONDENSED MATTER

J. Phys.: Condens. Matter **15** (2003) 4889–4902 PII: S0953-8984(03)60817-9

Second-harmonic generation and multiple mode effects in aperiodic optical superlattices with finite lateral width

Li-Ming Zhao[1], Ben-Yuan Gu[2,3], Yun-Song Zhou[1] and Fu-He Wang[1]

[1] Department of Physics, Capital Normal University, Beijing 100037, People's Republic of China
[2] CCAST (World Laboratory), PO Box 8730, Beijing 100080, People's Republic of China
[3] Institute of Physics, Academia Sinica, PO Box 603, Beijing 100080, People's Republic of China

E-mail: guby@aphy.iphy.ac.cn

Received 13 March 2003, in final form 22 April 2003
Published 11 July 2003
Online at stacks.iop.org/JPhysCM/15/4889

Abstract

We have studied second-harmonic generation (SHG) from quasi-one-dimensional aperiodic optical superlattices (AOSs) of finite lateral width by inverting poled ferroelectric domains. The search for optimal AOS structures corresponds with solving a difficult inverse source problem. We describe the design principle in real-space representation and undertake model designs. The numerical simulations show that the constructed AOSs can implement multiple-wavelength SHG with identical effective nonlinear coefficients at the pre-assigned wavelengths of the incident light. We investigate the effects of mode–mode coupling and the lateral width of the superlattice on the SHG for two cases: incident light beams of plane-wave and Gaussian profiles. When the number of modes increases, the effective nonlinear coefficient decreases in an oscillatory fashion at the beginning and then tends to a constant. For an incident plane-wave beam, the dependence of the effective nonlinear coefficient on the width of the sample is quite weak, while for an incident Gaussian beam this dependence exhibits a rapid decrease at the beginning and then tends to a constant. We display the variation in the effective nonlinear coefficients with the distance of propagation of the optical wave from where the incident light beam impinges on the sample surface and find that this variation exhibits monotonically increasing behaviour. This clearly infers that the contribution of every block to the optical SHG process takes the form of constructive addition. It is expected that this new design method may provide an effective and useful technique for constructing nonlinear optical material to match various practical applications.

1. Introduction

It is of importance to find laser sources at new wavelengths, and this can be achieved by nonlinear optical processes. The conventional method requires a phase-matching (PM) condition to obtain high conversion efficiency [1, 2]. However, the PM condition imposes a great restriction on the choice of the natural birefringent material. Another scheme is so-called quasi-phase matching (QPM) [3, 4]. This method can significantly diversify the class of nonlinear optical materials [5–13]. Some researchers successfully accomplished the design of an aperiodic optical superlattice (AOS) for multiple-wavelength second-harmonic generation (SHG) [14, 15]. The result of their design was recently confirmed by experiment [16]. However, previous studies were restricted only to one-dimensional AOS with an infinite lateral width [6, 14, 15]. In practical applications, the superlattice always possesses a finite lateral width. This situation usually occurs, as a high input power is adopted and the beam size is extended to avoid possible optical damage to the nonlinear crystal. Therefore, the effects of the finite lateral width of the AOS and the mode–mode coupling on the SHG could be interesting and important.

Motivated by the above work, in this paper we study the properties of SHG in an AOS with a finite lateral width, which can be fabricated by inverting poled ferroelectric domains. We first present the optimal design method for constructing the AOS. Then we carry out the specific design of an AOS that can implement multiple-wavelength SHG with identical effective nonlinear coefficients. In previous work, to guarantee the validity of the one dimensionality of the sample considered, it required that the size of the incident beam should be small compared to the lateral width of the sample. Therefore, an entrance aperture needs to be introduced. As a result, the energy of the incident light is cut off substantially. This leads to a lower SHG output power. If removing this limit on the aperture means that the SHG output is increased substantially, then it is favourable for practical applications. On the other hand, multiple-wavelength SHG with identical nonlinear coefficients in a single sample is very useful for serving as the light source of a colour display. Just one sample is then needed and the complex attenuator system can be avoided. We study the effects of the mode–mode coupling and the width of the superlattice on the SHG for two cases: incident light beams of plane-wave profile and Gaussian profile. We find that the effective nonlinear coefficient is decreased in an oscillatory fashion with an increase in the number of modes at the beginning, then tends to a constant. For an incident plane-wave beam, the effective nonlinear coefficient exhibits a weak dependence on width. However, for a Gaussian-profile incident beam, this dependence shows a rapid decrease at the beginning and then tends to a constant. We also display the contribution of each unit block of the sample to the SHG. This variation displays monotonically increasing behaviour. This clearly infers that the contribution of each block of the sample to the optical SHG process takes the form of constructive addition.

This paper is organized as follows. In section 2, we describe the design method and the formulas needed for the calculations. The calculated results are presented in section 3, together with analysis. Finally, a brief summary is given in section 4.

2. Theoretical formulas and design method

2.1. Formulas: effective nonlinear coefficient

The schematic configuration of the sample structure, which is surrounded by air, is shown in figure 1. The AOS with finite lateral width W is composed of laminar ferroelectric domains. The thickness of an individual domain can be different and is determined by special

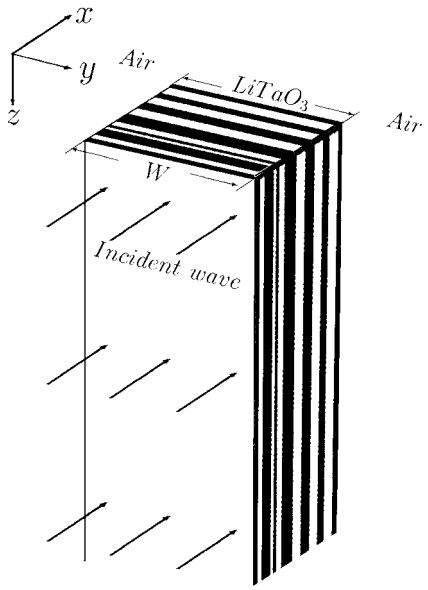

Figure 1. A schematic of the model structure of an AOS with finite lateral width. The structure is surrounded by air and the superlattice is composed of alternating laminar domains with positive polarization (black blocks) and negative polarization (white blocks) along the z axis. The incident plane wave is parallel to the xy plane and impinges on the sample perpendicularly. The size of the sample in the third direction is infinite and the related field component is of translational invariance.

optical parametric processes. This AOS has a quasi-one-dimensional (Q1D) modulation in the nonlinear coefficient along the direction normal to the domain layers. In order to use the largest nonlinear coefficient, d_{33}, of $LiTaO_3$ (LT) crystal, let the interfaces of the domains be parallel to the yz plane and the directions of propagation and polarization of the incident light be along the x and z axes, respectively. The size of the sample in the third direction (the z axis) is infinite with translational invariance.

We first discuss the SHG process for the case of a single wavelength. It is assumed that there is a laser beam with $\omega_1 = \omega$ incident normally from the left-hand side of the sample onto the surface of an AOS and that, through a nonlinear optical process, the second-harmonic wave (SHW) is generated. The AOS sample is illuminated fully by the fundamental wave (FW) in the lateral direction of the sample. The modulation of the nonlinear optical coefficient d_{33} in the AOS is described by $\chi(x) = \chi_j$ ($y \in [-W/2, W/2]$) in the jth unit block for $x_{j-1} \leqslant x \leqslant x_j$, and χ_j takes only a binary value, d_{33} and $-d_{33}$, corresponding to the positive and negative polarizations. We assume that $x_0 = 0$ and $x_N = L = N\Delta x$, where L denotes the thickness of the AOS sample, N is the number of the unit blocks in the sample, and Δx denotes the thickness of each individual unit block.

When considering the translational invariance of the sample along the z direction and the approximation of negligible pump power depletion, the electric field $E_{1\omega}(x, y)$ of the FW and the electric field $E_{2\omega}(x, y)$ of the SHW in the quasi-1D AOS satisfy the following homogeneous or inhomogeneous wave equation [2]:

$$\left(\frac{\mathrm{d}^2}{\mathrm{d}x^2} + \frac{\mathrm{d}^2}{\mathrm{d}y^2}\right) E_{1\omega}(x, y) + k_{1\omega}^2 E_{1\omega}(x, y) = 0, \tag{1}$$

$$\left(\frac{\mathrm{d}^2}{\mathrm{d}x^2}+\frac{\mathrm{d}^2}{\mathrm{d}y^2}\right)E_{2\omega}(x,y)+k_{2\omega}^2E_{2\omega}(x,y)=-k_{20}^2\chi(x)E_{1\omega}^2(x,y), \tag{2}$$

$$\chi(x)=|d_{33}|\tilde{d}(x), \tag{3}$$

where $\tilde{d}(x)$ only takes a binary value of 1 or -1. Outside the sample, i.e. in air, the fields of the FW (E_{1g}) and SHG (E_{2g}) satisfy the following equations:

$$\left(\frac{\mathrm{d}^2}{\mathrm{d}x^2}+\frac{\mathrm{d}^2}{\mathrm{d}y^2}\right)E_{1g}(x,y)+k_{10}^2E_{1g}(x,y)=0, \tag{4}$$

$$\left(\frac{\mathrm{d}^2}{\mathrm{d}x^2}+\frac{\mathrm{d}^2}{\mathrm{d}y^2}\right)E_{2g}(x,y)+k_{20}^2E_{2g}(x,y)=0. \tag{5}$$

The boundary conditions are:

$$\begin{aligned}
&E_{1\omega}\left(x,y=\pm\frac{W}{2}\right)=E_{1g}\left(x,y=\pm\frac{W}{2}\right),\\
&\frac{\partial E_{1\omega}}{\partial y}\left(x,y=\pm\frac{W}{2}\right)=\frac{\partial E_{1g}}{\partial y}\left(x,y=\pm\frac{W}{2}\right),\\
&E_{2\omega}\left(x,y=\pm\frac{W}{2}\right)=E_{2g}\left(x,y=\pm\frac{W}{2}\right),\\
&\frac{\partial E_{2\omega}}{\partial y}\left(x,y=\pm\frac{W}{2}\right)=\frac{\partial E_{2g}}{\partial y}\left(x,y=\pm\frac{W}{2}\right).
\end{aligned} \tag{6}$$

Here $k_{10}=\omega/c(k_{20}=2\omega/c)$ and $k_{1\omega}=n_{1\omega}\omega/c$ ($k_{2\omega}=n_{2\omega}k_{20}$), c is the light speed in vacuum, and $n_{1\omega}=n(\omega)$ ($n_{2\omega}=n(2\omega)$) is the refractive index of the material at the FW (SHW) frequency.

For the FW field, there are two types of mode. One is the guide mode, which is confined in the interior of the sample, and the other is the radiation mode. We only focus on the contribution of the guide mode to the SHG, because the energy of the radiation mode in the AOS is quite weak. To solve equation (1), we expand $E_{1\omega}(x,y)$ approximately in terms of transverse eigenmodes (see appendix):

$$\phi_{1n}(y)=\rho_{1n}\cos\left[\kappa_{1n}\left(y+\frac{W}{2}\right)-\mathrm{tg}^{-1}\left(\frac{\beta_{1n}}{\kappa_{1n}}\right)\right]$$

which satisfy the boundary conditions (6) as

$$E_{1\omega}(x,y)=\Sigma_n a_n\mathrm{e}^{\mathrm{i}p_{1n}x}\phi_{1n}(y), \tag{7}$$

where

$$\rho_{1n}=\sqrt{\frac{2}{W+\frac{\sin[2\mathrm{tg}^{-1}(\beta_{1n}/\kappa_{1n})]}{\kappa_{1n}}}+\frac{2\cos^2[\mathrm{tg}^{-1}(\beta_{1n}/\kappa_{1n})]}{\beta_{1n}}},$$

$p_{1n}^2=k_{1\omega}^2-\kappa_{1n}^2$, $\beta_{1n}^2=p_{1n}^2-k_{10}^2$, a_n is a constant expansion coefficient, and κ_{1n} and β_{1n} satisfy the following equation: $\kappa_{1n}=\frac{1}{W}[n\pi+2\mathrm{tg}^{-1}(\beta_{1n}/\kappa_{1n})]$. The solution of the inhomogeneous equation (2) can then be expressed in general as

$$E_{2\omega}(x,y)=\Sigma_n b_n(x)\mathrm{e}^{\mathrm{i}p_{2n}x}\phi_{2n}(y), \tag{8}$$

where p_{2n}, $\phi_{2n}(y)$ and κ_{2n} have similar forms of expression to p_{1n}, $\phi_{1n}(y)$ and κ_{1n}.

Substituting these formal solutions of equations (7) and (8) into (2) and considering the orthogonality and completeness of $\phi_{2n}(y)$ in the region $[-W/2, W/2]$, we obtain

$$\frac{\mathrm{d}^2 b_s(x)}{\mathrm{d}x^2} + 2\mathrm{i}p_{2s}\frac{\mathrm{d}b_s(x)}{\mathrm{d}x} = -k_{20}^2|d_{33}|\tilde{d}(x)\Sigma_{l,m}a_l a_m \mathrm{e}^{\mathrm{i}(p_{1l}+p_{1m}-p_{2s})x} \times \int_{-W/2}^{W/2} \mathrm{d}y\phi_{1l}(y)\phi_{1m}(y)\phi_{2s}(y). \tag{9}$$

Assuming a slowly varying amplitude of the SHW fields, i.e. $\mathrm{d}^2 b_s(x)/\mathrm{d}x^2 < 2\mathrm{i}p_{2s}\mathrm{d}b_s(x)/\mathrm{d}x$, we can thus derive

$$\frac{\mathrm{d}b_s(x)}{\mathrm{d}x} = \frac{\mathrm{i}k_{20}^2|d_{33}|\tilde{d}(x)}{2p_{2s}\sqrt{W}}\sum_{l,m} G_{lms}a_l a_m \mathrm{e}^{\mathrm{i}(p_{1l}+p_{1m}-p_{2s})x}. \tag{10}$$

Thus, its solution is

$$b_s(x) = \frac{\mathrm{i}k_{20}^2|d_{33}|L}{2p_{2s}\sqrt{W}}\sum_{l,m} G_{lms}a_l a_m F_{lms}(x), \tag{11}$$

where

$$F_{lms}(x) = \frac{1}{L}\int_0^x \mathrm{d}\zeta\, \tilde{d}(\zeta)\mathrm{e}^{\mathrm{i}(p_{1l}+p_{1m}-p_{2s})\zeta},$$

and G_{lms} is evaluated by

$$G_{lms} = \sqrt{W}\int_{-W/2}^{W/2} \mathrm{d}y\,\phi_{2s}(y)\phi_{1m}(y)\phi_{1l}(y) = \tfrac{1}{4}W^{3/2}\rho_{1m}\rho_{1l}\rho_{2s}\big\{\mathrm{sinc}\,[(\kappa_{1l}+\kappa_{1m}+\kappa_{2s})W/2] + \mathrm{sinc}\,[(\kappa_{1l}+\kappa_{1m}-\kappa_{2s})W/2] + \mathrm{sinc}\,[(\kappa_{1l}-\kappa_{1m}+\kappa_{2s})W/2] + \mathrm{sinc}\,[(\kappa_{1l}-\kappa_{1m}-\kappa_{2s})W/2]\big\}, \tag{12}$$

where $\mathrm{sinc}(y) = \sin(y)/y$. Substituting equation (11) into (8), we can calculate the SHW field at the right-hand exit of the sample:

$$E_{2\omega}(x = L, y) = \sum_{l,m,s}\frac{\mathrm{i}k_{20}^2|d_{33}|L}{2p_{2s}\sqrt{W}}G_{lms}a_l a_m \mathrm{e}^{\mathrm{i}p_{2s}L}\phi_{2s}(y)F_{lms}(L). \tag{13}$$

As discussed above, the distribution of fields in the z direction is uniform with the translational invariance. Therefore, we can take into account the light beam with a cross section of $S = W \times h$. Then, according to the definition of the intensity being the field energy density per unit area, the intensities of the SHW and FW are given by [2]

$$I_{2\omega} = P_{2\omega}/S = \left[\frac{1}{2Wh}\sqrt{\frac{\epsilon_{2\omega}}{\mu}}\int_0^h \mathrm{d}z\int_{-W/2}^{+W/2}\mathrm{d}y\,|E_{2\omega}(x = L, y)|^2\right] = \frac{1}{2W}\sqrt{\frac{\epsilon_{2\omega}}{\mu}}\Sigma_n|b_n(L)|^2, \tag{14}$$

$$I_{1\omega} = P_{1\omega}/S = \left[\frac{1}{2Wh}\sqrt{\frac{\epsilon_{1\omega}}{\mu}}\int_0^h \mathrm{d}z\int_{-W/2}^{+W/2}\mathrm{d}y\,|E_{1\omega}(x = 0, y)|^2\right] = \frac{1}{2W}\sqrt{\frac{\epsilon_{1\omega}}{\mu}}\Sigma_n|a_n|^2, \tag{15}$$

where $\epsilon_{1\omega,2\omega} = \epsilon_0 n_{1\omega,2\omega}^2$ and ϵ_0 is the permittivity of vacuum. Here we assume that the detector of the SHG is immediately attached to the exit of the sample. Finally, we can derive the conversion efficiency from the incident wave to the SHW as

$$\eta_{SHG} = \frac{8\pi^2|d_{33}|^2L^2}{c\epsilon_0\lambda^2 n_{2\omega}n_{1\omega}^2}I_{1\omega}\sum_{n,l_1,l_2,m_1,m_2}\frac{k_{2\omega}^2}{p_{2n}^2}A_{l_1}A_{l_2}^*A_{m_1}A_{m_2}^*G_{l_1m_1n}G_{l_2m_2n}F_{l_1m_1n}(L)F_{l_2m_2n}^*(L), \tag{16}$$

where $A_n = a_n/\sqrt{\sum_m |a_m|^2}$. It is evident that $|A|_n^2$ represents the relative weight of the nth-mode intensity in the FW.

For convenience, equation (16) can be rewritten as

$$\eta_{SHG} = C_s Q^2(\lambda)\xi_{eff}^{(s)}(\lambda) \tag{17}$$

with

$$C_s = \frac{8\pi^2|d_{33}|^2 I_{1\omega}L^2}{c\epsilon_0} \tag{18}$$

and

$$Q(\lambda) = \frac{1}{\lambda\sqrt{n_{2\omega}}n_{1\omega}}, \tag{19}$$

$$\xi_{eff}^{(s)}(\lambda) = \sum_{n,l_1,l_2,m_1,m_2}\left(\frac{k_{2\omega}^2}{p_{2n}^2}\right)A_{l_1}A_{l_2}^*A_{m_1}A_{m_2}^*G_{l_1m_1n}G_{l_2m_2n}F_{l_1m_1n}(L)F_{l_2m_2n}^*(L). \tag{20}$$

The total intensity of SHW at $x = L$ is

$$\begin{aligned} &I_{SHG} = 0.5\sqrt{\frac{\epsilon_{2\omega}}{\mu}}\Sigma_n|b_n(L)|^2 = W\eta_{SHG}I_{1\omega} = C_sQ^2(\lambda)I_{1\omega}[W\xi_{eff}^{(s)}(\lambda)] = R_{SHW}I_{1\omega}, \\ &R_{SHW} = I_{SHW}/I_{1\omega} = WC_sQ^2(\lambda)\xi_{eff}^{(s)}(\lambda), \end{aligned} \tag{21}$$

where, in principle, n, l_1, l_2, m_1, m_2 can take any integer number from 0 to ∞, but in practice they should be truncated to some finite values, according to the particular pattern of the incident FW field. Note that $\xi_{eff}^{(s)}(\lambda)$ represents the reduced effective nonlinear coefficient per area of sample for SHG and R_{SHW} expresses the ratio of the total SHW intensity to the FW one at the exit of sample.

The modes of the FW field depend strongly on the pattern of the incident light wave. As an example, we assume that a plane wave with $E = \exp(\mathrm{i}kx)$ ($y \in [-W/2, W/2]$) is incident normal to the surface of the sample. Its expansion coefficient can be evaluated as

$$\mathrm{e}^{\mathrm{i}kx}|_{x=0} = \sum_n a_n \mathrm{e}^{\mathrm{i}p_{1n}x}\phi_{1n}(y)|_{x=0},$$

therefore we obtain

$$a_n = \int_{-W/2}^{W/2}\mathrm{d}y\,\phi_{1n}(y) = \frac{2\rho_{1n}}{\kappa_{1n}}\sin\left(\frac{\kappa_{1n}W}{2}\right).$$

The nth mode weight of FW field is given by

$$A_n = \frac{2\rho_{1n}\sin(\kappa_{1n}W/2)}{\kappa_{1n}\sqrt{W}}, \tag{22}$$

where A_n has non-zero value only when $n = 0, 2, 4, 6, \ldots$.

For convenience, we define N_c (an even number) as the maximum mode index, i.e. taking $l_1, l_2, m_1, m_2 = 0, 2, 4, 6 \ldots N_c$ into account in the summation in equation (20), the contribution of the higher index modes can be negligible.

We now turn to discussing the more real experimental case when the incident light beam has the Gaussian profile $E = \mathrm{e}^{-y^2/\sigma^2}\exp(\mathrm{i}kx)$. The nth mode amplitude of the FW fields is given by

$$A_n = \rho_{1n}\int_{-W/2}^{W/2}\mathrm{d}y\,\mathrm{e}^{-y^2/\sigma^2}\phi_{1n}(y)\Big/\int_{-W/2}^{W/2}\mathrm{d}y\,\mathrm{e}^{-2y^2/\sigma^2}. \tag{23}$$

We can then derive an expression, analogous to equation (20), for the effective nonlinear coefficient of the SHG:

$$\xi_{eff}^{(s)'}(\lambda) = \frac{\sigma}{W}\xi_{eff}^{(s)}(\lambda). \tag{24}$$

2.2. Design method: simulation annealing approach

We now discuss the inverse source problem in constructing the optical AOS. It is assumed that the thickness of the unit block is Δx, thus the number of blocks in the sample is $N = L/\Delta x$. The position of each block is designated by $x_q = q\Delta x$, where $q = 0, 1, 2, 3 \ldots (N-1)$. We can then easily evaluate the integral equation (20):

$$\begin{aligned}
\xi_{eff}^{(s)}(\lambda) = & \sum_{n,l_1,l_2,m_1,m_2} \left(\frac{k_{2\omega}^2}{p_{2n}^2}\right) A_{l_1} A_{l_2}^* A_{m_1} A_{m_2}^* \\
& \times \left\{ G_{l_1 m_1 n} \frac{L}{N\Delta x} \Sigma_{q_1=0}^{N-1} \tilde{d}(x_{q_1}) [F_{l_1 m_1 n}(x_{q_1+1}) - F_{l_1 m_1 n}(x_{q_1})] \right\} \\
& \times \left\{ G_{l_2 m_2 n} \frac{L}{N\Delta x} \Sigma_{q_2=0}^{N-1} \tilde{d}(x_{q_2}) [F_{l_2 m_2 n}^*(x_{q_2+1}) - F_{l_2 m_2 n}^*(x_{q_2})] \right\} \\
= & \sum_{n,l_1,l_2,m_1,m_2} \left(\frac{k_{2\omega}^2}{p_{2n}^2}\right) A_{l_1} A_{l_2}^* A_{m_1} A_{m_2}^* \left\{ G_{l_1 m_1 n} \operatorname{sinc}[(p_{1l_1} + p_{1m_1} - p_{2n})\Delta x/2] \right\} \\
& \times \left\{ \frac{1}{N} \sum_{q_1=0}^{N-1} \tilde{d}(x_{q_1}) \exp[\mathrm{i}(p_{1l_1} + p_{1m_1} - p_{2n})(q_1 + 0.5)\Delta x] \right\} \\
& \times \left\{ G_{l_2 m_2 n} \operatorname{sinc}[(p_{1l_2} + p_{1m_2} - p_{2n})\Delta x/2] \right\} \\
& \times \left\{ \frac{1}{N} \sum_{q_2=0}^{N-1} \tilde{d}(x_{q_2}) \exp[-\mathrm{i}(p_{1l_2} + p_{1m_2} - p_{2n})(q_2 + 0.5)\Delta x] \right\}. \qquad (25)
\end{aligned}$$

It is clearly seen that $\xi_{eff}^{(s)}(\lambda)$ is governed by three factors:

(i) First, the factor $\sum_{l,m} A_l A_m G_{lmn}$ reflects the coupling between the transverse modes of the FW. The finite width of the superlattice leads to a non-uniform distribution of both the FW and SHW fields in the lateral direction of the sample. The coupling between the transverse modes of the FW can generate a large amount of SHW transverse modes. From the numerical simulation of the term $\sum_{l,m} A_l A_m G_{lmn}$, it is found that, if the mode index of the SHW is high enough, the contribution of these higher-index modes to $\xi_{eff}^{(s)}(\lambda)$ is quite small. Thus, only the transverse modes of the SHW with lower index bring a major contribution to $\xi_{eff}^{(s)}(\lambda)$.

(ii) The second factor is a sinc function, such as $\operatorname{sinc}[(p_{1l} + p_{1m} - p_{2n})\Delta x/2]$. This is associated closely with the unit block in the sample and depends strongly on Δx as well as the coherence length $l_c^s(\lambda)$ [$l_c^s(\lambda) = 2\pi/\Delta k = 2\pi/(p_{2n} - p_{1m} - p_{1l})$].

(iii) The third factor, $(1/N)\sum_{q=0}^{N-1}(-1)^q \exp[\mathrm{i}(p_{1l} + p_{1m} - p_{2n})(q + 0.5)\Delta x]$, reflects the interference of the generating wave from the individual block and depends on the configuration of domains and the phase lag of the generating wave from the individual block of the sample.

The optimal design of the AOS for SHG can be described as a search for the maximum of $\xi_{eff}^{(s)}(\lambda)$ with respect to $\tilde{d}(q\Delta x)$. Taking the second factor into consideration, the maximum-value condition demands $\Delta x = [(2m+1)/2] l_c^s(\lambda)$, where $m = 0, 1, 2, \ldots$, and the maximum value of this factor is $2/[\pi(2m+1)]$. The maximum-value condition for the second factor corresponds to perfectly constructive interference. For the case of a periodic structure with a period of $a = 2\Delta x$, $\tilde{d}(x_q)$ just takes the value of $\tilde{d}(q\Delta x) = (-1)^q$ for $q = 0, 1, 2 \ldots (N-1)$. We thus obtain

$$\frac{1}{N} \sum_{q=0}^{N-1} (-1)^q \exp[\mathrm{i}(p_{1l} + p_{1m} - p_{2n})(q + 0.5)\Delta x] = 1. \qquad (26)$$

However, for an optical superlattice of finite lateral width, the above condition cannot be satisfied exactly due to the existence of multiple modes for both FW and SHW. It is noted that only the lower index modes of the SHW or FW provide major contributions, as addressed before. In an ideal case, the phase-lagging factor perfectly matches the reversal of the orientation between two adjacent blocks and perfect constructive interference occurs. However, in the case of the AOS, the situation becomes much more complicated and an inverse source problem must be solved. Such an optimal nonlinear problem can be solved by using the simulated annealing (SA) method [17, 18] in which an objective function D should be minimized, and then a favourable orientation of each domain layer in the sample can be determined completely.

To demonstrate the effectiveness and usefulness of the SA method in dealing with the inverse source problem, we consider the case of a single-wavelength SHG to verify the SA method available. To be compatible with generality, we consider the case of multiple modes, $N_c = 10$, in the SA algorithm. We choose the parameters to be: the wavelength of the incident beam $\lambda = 1.06\ \mu$m; the width of the superlattice $W = 1.0$ mm; the thickness of the unit block $\Delta x = l_c^{(s)}/2 = \pi/(k_{2\omega} - 2k_\omega) = 3.8713\ \mu$m; and the number of blocks 10^3. Thus, the total thickness of the sample is $L = 3.871$ mm. The refractive index of the material at the FW (SHW) frequency is evaluated using the Sellmeier equation given in [8]. The objective function used in the SA is chosen to be

$$D = |\xi^0 - \xi_{eff}^{(s)}(\lambda)|, \tag{27}$$

where ξ^0 is a pre-designated value in guiding the SA procedure and $\xi_{eff}^{(s)}(\lambda)$ is given in equation (20). Finally, we obtain a perfect periodic structure with a period of $a = 2\Delta x = l_c^{(s)}(\lambda)$, as expected. The reduced effective nonlinear coefficient of $\xi_{eff}^{(s)}(\lambda)$ is 0.4322. The results that are obtained strongly support the SA method as being appropriate for dealing with the above-mentioned inverse source problem.

3. Results and analysis

We now undertake a specific design of the AOS that accomplishes multiple-wavelength SHG with an identical effective nonlinear coefficient $\xi_{eff}^{(s)}(\lambda) = \xi^{(0)}$. First, we have to choose carefully an appropriate thickness Δx of the unit block, which is mainly determined from the maximum value of the sinc function $\mathrm{sinc}\,[(p_{1l} + p_{1m} - p_{2n})\Delta x/2]$. This factor depends strongly on wavelength. As is well known, $\mathrm{sinc}\,(x) \sim 1$ when x is small enough, thus this wavelength dependence can be negligible. Therefore, we choose $\Delta x = 3\ \mu$m for compatibility with state-of-the-art micro-fabrication. The objective function used in the SA method is now chosen to be

$$D = \Sigma_\alpha[|\xi^{(0)} - \xi_{eff}^{(s)}(\lambda_\alpha)|] + \gamma[\max\{\xi_{eff}^{(s)}(\lambda_\alpha)\} - \min\{\xi_{eff}^{(s)}(\lambda_\alpha)\}], \tag{28}$$

where the symbol $\max\{\cdots\}(\min\{\cdots\})$ means taking the maximum (minimum) value among all the quantities included in $\{\cdots\}$, γ is an adjustable parameter that takes a value of 0.3–3.0, and λ_α is set to the values 0.9720, 1.0820, 1.2830, 13940 and 1.5687 μm. The dispersion relation of the refractive indices of the LT crystal at the FW and SHW frequencies is calculated at $T = 25\,^\circ$C according to the Sellmeier formula given in [8].

We calculate the effective nonlinear coefficient for the cases of a single mode and multiple modes of the incident FW beam with a plane-wave profile. As the parameters in the calculations, we adopt a total thickness of sample $L = 3.0$ mm, the number of blocks $N = 10^3$, and the superlattice width $W = 1.0$ mm. Figure 2(a) shows a grey-scale diagram of the constructed AOS in part for the case of multiple modes of $N_c = 10$. The black (white)

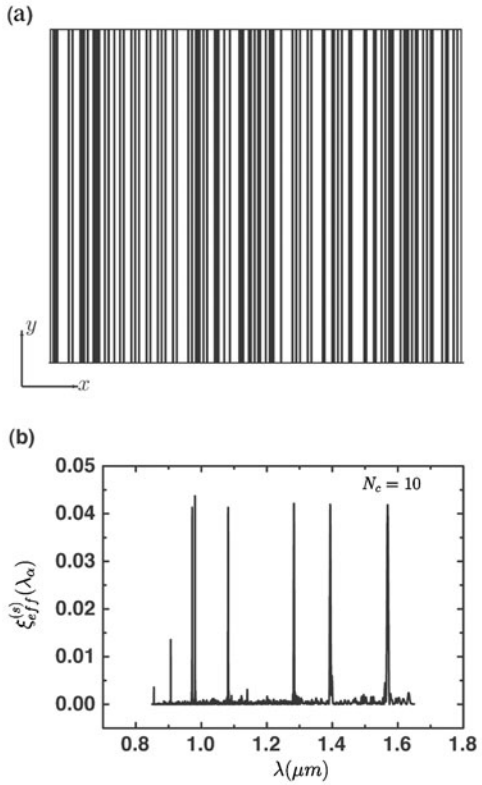

Figure 2. The characteristics of the constructed AOS that can implement multiple-wavelengths SHG with identical nonlinear coefficients. The number of modes of the incident FW field involved in the optical design of the AOS is $N_c = 10$. (a) A grey-scale diagram representing the domain orientation of the specific AOS in part (black blocks correspond to positive polarization; white blocks to negative polarization). (b) The wavelength dependence of $\xi^{(s)}_{eff}(\lambda)$.

strip represents the positive (negative) polarization domain. Figure 2(b) displays the calculated reduced effective nonlinear coefficient in the case of $N_c = 10$ as a function of wavelength of the FW. After scanning a wide range of wavelengths from 0.85 to 1.65 μm with a resolution of 0.5 Å, it exhibits peaks of almost identical height at the pre-assigned wavelengths. It is also seen that one unexpected peak of $\lambda = 0.980\,95$ μm appears near the pre-set wavelength of $\lambda = 0.972\,00$ μm.

Table 1 shows the calculated effective nonlinear coefficient at the five pre-assigned wavelengths of the FW for the cases $N_c = 0, 2, 4, 6$ and 8. It is evident that, for the case of $N_c = 0$, the average value of $\xi^{(s)}_{eff}(\lambda_\alpha)$ is 0.049 32 and the non-uniformity defined by $\Delta\xi^{(s)}_{eff} = (1/\alpha)[\sum_\alpha |\xi^{(s)}_{eff}(\lambda_\alpha) - \langle\xi^{(s)}_{eff}\rangle|/\langle\xi^{(s)}_{eff}\rangle]$ equals 0.203%. Also, for $N_c = 2$ (4, 6 and 8), the average value of $\xi^{(s)}_{eff}(\lambda_\alpha)$ is 0.042 86 (0.042 68, 0.041 59 and 0.039 99), and the non-uniformity is 0.0653 (0.276, 0.303 and 0.245%).

Figure 3 displays the variations in the calculated effective nonlinear coefficient at the pre-assigned five wavelengths of the FW with N_c for values of several W. The widths of the superlattice are 1.0, 2.0 and 2.5 mm. It is clear that the $\langle\xi^{(s)}_{eff}\rangle$ is basically decreased containing some oscillations when increasing the number of transverse modes of FW.

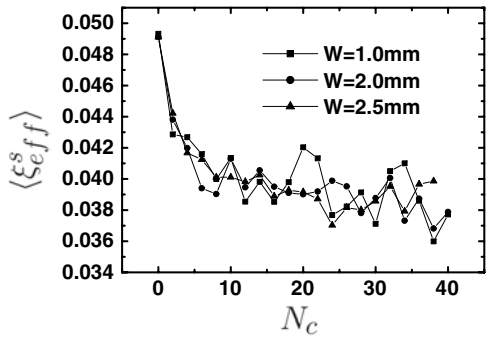

Figure 3. The variation of $\langle \xi^{(s)}_{eff} \rangle$ with the number of modes of the FW for several widths of the AOS sample, $W = 1.0$, 2.0 and 2.5 mm, for the case of a plane-wave incident beam. N_c is the maximum mode index of the FW field.

Table 1. The effective nonlinear coefficient $\xi^{(s)}_{eff}(\lambda)$ at the five pre-assigned wavelengths of the FW for the cases $N_c = 0$, 2, 4, 6 and 8 ($W = 1.0$ mm).

λ (μm)	$\xi^{(s)}_{eff}(\lambda)(N_c = 0)$	$\xi^{(s)}_{eff}(\lambda)(N_c = 2)$	$\xi^{(s)}_{eff}(\lambda)(N_c = 4)$	$\xi^{(s)}_{eff}(\lambda)(N_c = 6)$	$\xi^{(s)}_{eff}(\lambda)(N_c = 8)$
0.9720	0.049 28	0.042 86	0.042 62	0.041 58	0.039 75
1.0820	0.049 20	0.042 91	0.042 61	0.041 77	0.040 06
1.2830	0.049 22	0.042 84	0.042 59	0.041 72	0.040 15
1.3940	0.049 38	0.042 87	0.042 81	0.041 43	0.040 03
1.5687	0.049 50	0.042 80	0.042 92	0.041 44	0.040 00

$\xi^{(s)}_{eff}(\lambda_\alpha)$ depends strongly on the field distribution of FW. The interference effect between the modes may change the distribution of the field. From equation (22), the following results can be deduced from the numerical simulation:

(i) The phase of the contribution from the two connective modes is inverse. This leads to the result that the variation of the intensity of FW with N_c is not always decreasing monotonically.
(ii) The higher-index modes correspond to nonzero small components of the FW, so the decrease in $\xi^{(s)}_{eff}(\lambda_\alpha)$ with N_c cannot approach zero but rather a finite value, as seen in figure 3.

It is interesting to show the effect of the width of the superlattice on the SHG. It is seen clearly from figure 3 that the change in $\langle \xi^{(s)}_{eff} \rangle$ for different widthes of the sample is quite small, even if $W \to \infty$. These results can be well understood: as the incident energy per area of the FW retains a fixed value, the variation in $\langle \xi^{(s)}_{eff} \rangle$ with width is weak. In contrast, R_{SHW} is the ratio of the total SHW intensity to the FW one at the exit of the sample, so it is roughly proportional to the width of sample, as expected.

It is worth pointing out that, for the one-dimensional AOS sample of infinite width, to avoid the boundary effect the width of the incident light beam must be small compared to the lateral width of the sample. Thus the SHW's total energy becomes relatively low due to the limited width of the incident light beam.

To further reveal the characteristics of SHG in the constructed AOS, figure 4 displays the variation in $\xi^{(s)}_{eff}(\lambda)$ with the distance of propagation of the optical wave, x, from where the incident light beam impinges on the sample surface for the five pre-assigned wavelengths of the

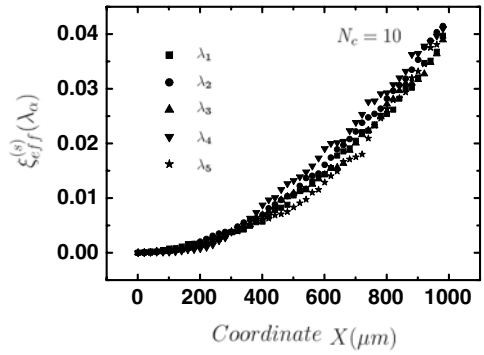

Figure 4. The variation in $\xi^{(s)}_{eff}(\lambda)$ with the propagating distance of the incident optical wave in the AOS sample in figure 2 for five pre-assigned wavelengths of the FW.

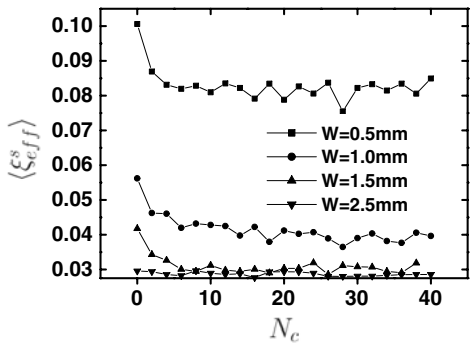

Figure 5. As for figure 3, except that the incident light beam is of Gaussian profile.

FW. It is apparent that all the curves exhibit increasing behaviour as well as an almost identical rising slope. This implies that the orientation of domains is quite favourable to the SHG process, because the contribution of successive blocks to $\xi^{(s)}_{eff}(\lambda)$ is constructive accumulation.

We now consider the more real experimental case: an incident light beam of Gaussian profile of $E = \mathrm{e}^{-y^2/\sigma^2}\exp(\mathrm{i}kx)$. Figure 5 shows the dependence of the effective nonlinear coefficient at the pre-assigned wavelengths of the FW: N_c, for several different widths of the sample, $W = 0.5, 1.0, 1.5$ and 2.5 mm. The other parameters are as follows: $\Delta x = 3$ μm; $L = 3.0$ mm; $N = 10^3$; and $\sigma = 1.0$ mm. The behaviour is similar to figure 3. However, for a given N_c, as increasing W, $\langle \xi^{(s)}_{eff} \rangle$ is decreased rapidly at the beginning and then tends to a constant. These results can be interpreted well: for the Gaussian profile beam, the light energy is focused mostly within the range of σ. When the width W of the sample is smaller than $\sigma = 1.0$ mm, for example $W = 0.5$ mm, the average intensity of the incident FW beam that is involved in the SHG process is relatively large at the entry of the sample. Thus the corresponding plateau value of $\langle \xi^{(s)}_{eff} \rangle$ should be large. However, when increasing the width of the sample, the average intensity of the incident FW beam is decreased accordingly. Thus the plateau value of the $\langle \xi^{(s)}_{eff} \rangle$ is reduced. However, when $W > \sigma$, the intensity of the incident FW beam almost retains a small change with W because most of the energy of the incident FW beam is focused within the range of σ. As a result, the variation in the plateau value of $\langle \xi^{(s)}_{eff} \rangle$ with W now becomes quite weak, as shown by the curves corresponding to $W = 1.5$ and 2.5 mm in figure 5.

4. Summary

We have investigated the characteristics of SHG from an AOS with finite lateral width, as is necessary for extending incident light beams to avoid possible damage to a nonlinear crystal when high input power is adopted. The optimal design of the AOS for SHG corresponds to a difficult inverse problem in nonlinear optics. To deal with this problem we employ the SA method. We describe the idea of the design and carry out the model designs. For example, the constructed AOS can achieve multiple-wavelength SHG with identical effective nonlinear coefficients at the pre-assigned multiple wavelengths. We study the effects of mode–mode coupling between the transverse modes of the FW and SHW and the lateral width of the sample on $\xi_{eff}^{(s)}(\lambda)$ for both cases of incident light beams of plane-wave and Gaussian profile.

$\xi_{eff}^{(s)}(\lambda)$ is decreased with an increase in the number of transverse modes. $\xi_{eff}^{(s)}(\lambda)$ is insensitive to the change of the width W of the AOS sample for the incident plane-wave beam, However, for the incident Gaussian profile beam, the W dependence of $\xi_{eff}^{(s)}(\lambda)$ exhibits rapidly decreasing behaviour at the beginning and then tends to a constant. We also show the variation of the effective nonlinear optical coefficient with the distance of propagation of the optical wave from where the incident light beam impinges on the sample surface, and we find that it displays monotonically increasing behaviour. This clearly confirms that the contribution of every individual block in the sample to the optical parametric process is a constructive accumulation. We believe that our proposed design method may provide an instructive and useful method for making new nonlinear optical materials compatible with various practical applications.

Acknowledgments

This work was supported by the Chinese National Key Basic Research Special Fund and by the Natural Science Foundation of Beijing, China.

Appendix

In this appendix, we provide a detailed derivation of the transverse eigenmodes of the FW in the AOS sample of finite width.

The electric field $E_{1\omega}(x, y)$ of the FW satisfies the following wave equations:

$$\left(\frac{\mathrm{d}^2}{\mathrm{d}x^2} + \frac{\mathrm{d}^2}{\mathrm{d}y^2}\right) E_{1\omega}(x, y) + k_{1\omega}^2 E_{1\omega}(x, y) = 0, \qquad \text{inside the AOS} \tag{A.1}$$

$$\left(\frac{\mathrm{d}^2}{\mathrm{d}x^2} + \frac{\mathrm{d}^2}{\mathrm{d}y^2}\right) E_{1g}(x, y) + k_{10}^2 E_{1g}(x, y) = 0, \qquad \text{in air.} \tag{A.2}$$

The boundary conditions are

$$\begin{aligned} &E_{1\omega}\left(x, y = \pm\frac{W}{2}\right) = E_{1g}\left(x, y = \pm\frac{W}{2}\right), \\ &\frac{\partial E_{1\omega}}{\partial y}\left(x, y = \pm\frac{W}{2}\right) = \frac{\partial E_{1g}}{\partial y}\left(x, y = \pm\frac{W}{2}\right). \end{aligned} \tag{A.3}$$

Here $k_{10} = \omega/c$ and $k_{1\omega} = n_{1\omega}\omega/c$, where c is the light speed in vacuum and $n_{1\omega} = n(\omega)$ is the refractive index of the material at the FW frequency.

There are two cases in solving equations (A.1) and (A.2):

$$(i) \quad k_{10}^2 < p_{1n}^2 < k_{1\omega}^2 \qquad \text{(corresponding to the guide wave),} \tag{A.4a}$$

$$(ii) \quad p_{1n}^2 < k_{10}^2 \qquad \text{(corresponding to the radiation wave)}, \tag{A.4b}$$

where p_{1n} represents the wavevector of the FW along the x axis. We define $p_{1n}^2 = k_{1\omega}^2 - \kappa_{1n}^2$ and $\beta_{1n}^2 = p_{1n}^2 - k_{10}^2$ for the guide waves and $\beta_{1n}^2 = k_{10}^2 - p_{1n}^2$ for the radiation waves.

The formal solution of equation (A.1) can be written as

$$E_{1\omega}(x, y) = [f_1 \cos(\kappa_{1n} y) + f_2 \sin(\kappa_{1n} y)]\mathrm{e}^{\mathrm{i}p_{1n}x}. \tag{A.5}$$

For the case of the guide modes, we assume the formal solution to equation (A.2) to be

$$E_{1g}(x, y) = \begin{cases} g_1 \exp\left[\beta_{1n}\left(y - \dfrac{W}{2}\right)\right]\mathrm{e}^{\mathrm{i}\tau x}, & y \leqslant -W/2, \\ g_2 \exp\left[-\beta_{1n}\left(y + \dfrac{W}{2}\right)\right]\mathrm{e}^{\mathrm{i}\tau x}, & y \geqslant W/2. \end{cases} \tag{A.6}$$

After imposing the boundary conditions and through the standard tedious manipulations, we can obtain the related transverse eigenmodes of the FW. The field distribution of the FW possesses even or odd symmetry, due to the symmetry of the sample structure.

For the even symmetric solution, we obtain a set of bases that satisfy orthogonality and completeness, i.e.

$$\varphi_{1n}(y) = \begin{cases} f_1 \cos(\kappa_{1n} y), & y \in [-W/2, W/2], \\ g_1 \exp\left[-\beta_{1n}\left(y + \dfrac{W}{2}\right)\right], & y \in [W/2, \infty], \\ g_1 \exp\left[\beta_{1n}\left(y - \dfrac{W}{2}\right)\right], & y \in [-\infty, -W/2] \end{cases}$$

where $f_1 = \sqrt{2}\big[W + \frac{\sin(\kappa_{1n}W)}{\kappa_{1n}} + \frac{2\cos^2(\kappa_{1n}W/2)}{\beta_{1n}}\big]^{-\frac{1}{2}}$, as determined by the normalized condition; $g_1 = f_1 \cos(\kappa_{1n}W/2)\mathrm{e}^{\beta_{1n}W}$, $\kappa_{1n} = \frac{1}{W}\big[2n\pi + 2\,\mathrm{tg}^{-1}\big(\frac{\beta_{1n}}{\kappa_{1n}}\big)\big]$.

For the odd symmetric solution, we have

$$\varphi_{1n}(y) = \begin{cases} f_2 \sin(\kappa_{1n} y), & y \in [-W/2, W/2], \\ g_1 \exp\left[-\beta_{1n}\left(y + \dfrac{W}{2}\right)\right], & y \in [W/2, \infty], \\ -g_1 \exp\left[\beta_{1n}\left(y - \dfrac{W}{2}\right)\right], & y \in [-\infty, -W/2], \end{cases}$$

with $f_2 = \sqrt{2}\big[W - \frac{\sin(\kappa_{1n}W)}{\kappa_{1n}} + \frac{2\sin^2(\kappa_{1n}W/2)}{\beta_{1n}}\big]^{-\frac{1}{2}}$, $g_1 = -f_2 \sin(\kappa_{1n}W/2)\mathrm{e}^{\beta_{1n}W}$, $\kappa_{1n} = \frac{1}{W}\big[(2n-1)\pi + 2\,\mathrm{tg}^{-1}\big(\frac{\beta_{1n}}{\kappa_{1n}}\big)\big]$. Through the standard manipulations of trigonometrical function algebra, $\phi_{1n}(y)$ in the AOS region can be unified as a single cosine function, as shown in the text.

We now study the case of the radiation modes and assume that the formal solution for equation (A.2) is

$$E_{1g}(x, y) = \begin{cases} [u_1 \cos(\beta_{1n} y) + v_1 \sin(\beta_{1n} y)]\mathrm{e}^{\mathrm{i}\tau x}, & y \in [W/2, \infty], \\ [u_2 \cos(\beta_{1n} y) + v_2 \sin(\beta_{1n} y)]\mathrm{e}^{\mathrm{i}\tau x}, & y \in [-\infty, -W/2]. \end{cases}$$

After imposing the boundary conditions, we obtain the corresponding solutions. When the field distribution possesses even symmetry ($u_1 = u_2$, $v_1 = -v_2$), the corresponding solution is

$$\varphi_{1n}(y) = \begin{cases} f_1 \cos(\kappa_{1n} y), & y \in [-W/2, W/2], \\ u_1 \cos(\beta_{1n} y) + v_1 \sin(\beta_{1n} y), & y \in [W/2, \infty], \\ u_1 \cos(\beta_{1n} y) - v_1 \sin(\beta_{1n} y), & y \in [-\infty, -W/2], \end{cases}$$

where

$$u_1 = \left(\frac{f_1}{\beta_{1n}}\right)\left[\beta_{1n}\cos\left(\frac{\kappa_{1n}W}{2}\right)\cos\left(\frac{\beta_{1n}W}{2}\right) + \kappa_{1n}\sin\left(\frac{\kappa_{1n}W}{2}\right)\sin\left(\frac{\beta_{1n}W}{2}\right)\right],$$

$$v_1 = \left(\frac{f_2}{\beta_{1n}}\right)\left[\beta_{1n}\cos\left(\frac{\kappa_{1n}W}{2}\right)\sin\left(\frac{\beta_{1n}W}{2}\right) - \kappa_{1n}\sin\left(\frac{\kappa_{1n}W}{2}\right)\cos\left(\frac{\beta_{1n}W}{2}\right)\right],$$

and κ_{1n} and β_{1n} satisfy the equation

$$\mathrm{tg}\left(\frac{\kappa_{1n}W}{2}\right) = \left(\frac{\beta_{1n}}{\kappa_{1n}}\right)\frac{u_1\sin\left(\frac{\beta_{1n}W}{2}\right) - v_1\cos\left(\frac{\beta_{1n}W}{2}\right)}{u_1\cos\left(\frac{\beta_{1n}W}{2}\right) + v_1\sin\left(\frac{\beta_{1n}W}{2}\right)}.$$

When the field distribution possesses odd symmetry ($u_1 = -u_2, v_1 = v_2$), the corresponding solution is

$$\varphi_{1n}(y) = \begin{cases} f_2\sin(\kappa_{1n}y), & y \in [-W/2, W/2], \\ u_1\cos(\beta_{1n}y) + v_1\sin(\beta_{1n}y), & y \in [W/2, \infty], \\ -u_1\cos(\beta_{1n}y) + v_1\sin(\beta_{1n}y), & y \in [-\infty, -W/2], \end{cases}$$

where

$$u_1 = \left(\frac{f_2}{\beta_{1n}}\right)\left[\beta_{1n}\sin\left(\frac{\kappa_{1n}W}{2}\right)\cos\left(\frac{\beta_{1n}W}{2}\right) - \kappa_{1n}\cos\left(\frac{\kappa_{1n}W}{2}\right)\sin\left(\frac{\beta_{1n}W}{2}\right)\right],$$

$$v_1 = \left(\frac{f_2}{\beta_{1n}}\right)\left[\beta_{1n}\sin\left(\frac{\kappa_{1n}W}{2}\right)\sin\left(\frac{\beta_{1n}W}{2}\right) + \kappa_{1n}\cos\left(\frac{\kappa_{1n}W}{2}\right)\cos\left(\frac{\beta_{1n}W}{2}\right)\right],$$

κ_{1n} and β_{1n} satisfy the equation

$$\mathrm{ctg}\left(\frac{\kappa_{1n}W}{2}\right) = -\left(\frac{\beta_{1n}}{\kappa_{1n}}\right)\frac{u_1\sin\left(\frac{\beta_{1n}W}{2}\right) - v_1\cos\left(\frac{\beta_{1n}W}{2}\right)}{u_1\cos\left(\frac{\beta_{1n}W}{2}\right) + v_1\sin\left(\frac{\beta_{1n}W}{2}\right)}.$$

We learn from the numerical analysis that the values of β_{1n} and κ_{1n} are discrete for the guide modes. The total number of guide modes, which are determined by equation (A.4*a*), is finite. κ_{1n} is increased with the increase in the mode index n. However, β_{1n} is decreased. For the radiation modes, the values of β_{1n} and κ_{1n} are continuous. Therefore, only part of the FW's energy can be converted to the SHG. Consequently, the corresponding conversion efficiency is quite low.

References

[1] Yariv A and Yeh P 1984 *Optical Wave in Crystal* (New York: Wiley) p 504
[2] Shen Y R 1984 *The Principles of Nonlinear Optics* (New York: Wiley)
[3] Bloembergen N and Sievers A J 1970 *Appl. Phys. Lett.* **17** 483
[4] Armstrong A, Bloembergen N, Ducuing J and Pershan P S 1962 *Phys. Rev.* **127** 1918
[5] Zhu S N, Zhu Y Y and Ming N B 1997 *Science* **278** 843
[6] Zhu S N, Zhu Y Y, Qin Y Q, Wang H F, Ge C Z and Ming N B 1997 *Phys. Rev. Lett.* **78** 2752
[7] Zhu S N, Zhu Y Y, Zhang Z Y, Shu H, Wang H F, Hong J F, Ge C Z and Ming N B 1995 *J. Appl. Phys.* **77** 5481
[8] Meyn J P and Fejer M M 1997 *Opt. Lett.* **22** 1214
[9] Miller G D, Batchko R G, Tulloch W M, Weise D R, Fejer M M and Ber R L 1997 *Opt. Lett.* **22** 1834
[10] Feng D, Ming N B, Hong J H, Yang Y S, Zhu J S, Yang Z and Wang Y N 1980 *Appl. Phys. Lett.* **37** 607
[11] Xue Y H, Ming N B, Zhu J S and Feng D 1983 *Acta Phys. Sin.* **32** 1515 (Engl. transl. 1984 *Chin. Phys.* **4** 554)
[12] Thompson D E, McMullen J D and Anderson D B 1973 *Appl. Phys. Lett.* **29** 113
[13] Deway C F and Hocker L O 1975 *Appl. Phys. Lett.* **26** 442
[14] Gu B Y, Dong B Z, Zhang Y and Yang G Z 1999 *Appl. Phys. Lett.* **75** 2175
[15] Gu B Y, Zhang Y and Dong B Z 2000 *J. Appl. Phys.* **87** 7629
[16] Lee Y W, Fan F C, Huang Y C, Gu B Y, Dong B Z and Chou M H 2002 *Opt. Lett.* **27** 2191
[17] Kirkpatrick S, Gelatt C D and Vecchi M P 1983 *Science* **220** 671
[18] Kirkpatrick S 1983 *J. Stat. Phys.* **34** 975